ENHANCED STRAIN RESISTANCE OF FRACTAL FIBER LASER-INDUCED GRAPHENE FOR FLEXIBLE ELECTRODES VIA ANNEALING AND PLASMA ETCHING

Yanru Chen[1,2], Jiaqi Liu[1], Yixin Liu[1],and Min Zhang[1]*
[1] Shenzhen International Graduate School, Tsinghua University, CHINA and
[2] Electrical and Computer Engineering Department, University of California San Diego, USA

2025 23rd International Conference on Solid-State Sensors, Actuators and Microsystems (Transducers) | 979-8-3315-1381-8/25/$31.00 ©2025 IEEE | DOI: 10.1109/TRANSDUCERS61432.2025.11109269

ABSTRACT

Laser-induced graphene (LIG) is a promising material for flexible and stretchable electronics due to its porous structure and high electrical conductivity. However, its mechanical fragility under strain limits practical applications. Here, we present a simple yet effective dual-treatment method, low-temperature annealing at 180°C followed by oxygen plasma etching—to enhance LIG's strain resistance. This process induces a dense fractal fiber network that preserves conductivity while improving structural stability. The treated LIG exhibits a reduced gauge factor (GF) of 7.43, approximately half that of untreated LIG, indicating lower sensitivity to strain-induced resistance changes. Scanning electron microscopy (SEM), Raman spectroscopy, and X-ray photoelectron spectroscopy (XPS) analyses reveal improved fiber connectivity, enhanced graphitization, and reduced oxygen defects. The method is scalable, substrate-friendly, and well-suited for high-performance stretchable electronics.

KEYWORDS

Laser-induced graphene, Fractal microstructure, Strain-resistant electrodes, Annealing and plasma etching, Flexible electronics.

INTRODUCTION

Flexible electronics, wearable sensors, and soft devices require electrode materials that are both highly conductive and mechanically robust under deformation. Laser-induced graphene (LIG), formed by direct infrared laser scribing of carbon-rich substrates [1] such as polyimide (PI), has emerged as a promising candidate due to its excellent conductivity, porous 3D network, and mask-free, transfer-free fabrication process [2–4].

However, conventional LIG structures often suffer from mechanical fragility under strain, leading to cracking, fiber delamination, and resistance instability during repeated bending or stretching [5,6]. To overcome these limitations, a variety of enhancement strategies have been explored, including chemical doping [7], metallic or oxide nanoparticle incorporation [8,9], multilayer or sandwich structures [10,11], and fractal or biomimetic topological patterning [12,13]. However, these methods often rely on complex fabrication steps or toxic additives, limiting scalability. Recently, post-treatment techniques have attracted increasing attention as a scalable and cleaner alternative for improving LIG's microstructural resilience. Flash thermal annealing improves conductivity by reorganizing the sp^2 network [6], while femtosecond laser processing produces highly crystalline LIG [14], but its rigidity limits strain tolerance in flexible electrodes. Additionally, integration with stretchable elastomers [7,10] and pattern designs inspired by natural structures [12,13] further improves stretchability, but trade-offs between conductivity and durability remain.

We propose a simple, scalable dual-treatment approach combining low-temperature annealing and oxygen plasma etching to address the persistent challenge of balancing conductivity and mechanical stability. This process promotes fiber densification, removes weakly bonded amorphous carbon, and forms an interconnected fractal fiber network. Our treated LIG maintains high conductivity while significantly improving strain resistance. Through scanning electron microscopy (SEM), Raman spectroscopy, and X-ray photoelectron spectroscopy (XPS) analyses, as well as gauge factor and transfer testing, we demonstrate that this dual-treatment strategy offers a robust route to reliable, strain-tolerant LIG electrodes for next-generation stretchable electronics.

FABRICATION AND CHARACTERIZATION

LIG Fabrication and Post-Treatment

Commercial polyimide (PI, Kapton) sheets with a thickness of 125 μm were used as substrates. Before laser processing, the PI films were cleaned by sequential ultrasonic rinsing in isopropyl alcohol and deionized water for 10 minutes each, followed by nitrogen drying. The cleaned PI sheets were then affixed onto 6-inch silicon wafers using a thin polydimethylsiloxane (PDMS) adhesive layer to ensure flatness and eliminate air bubbles during laser scribing.

LIG patterns (6 mm × 6 mm) were generated using a CO_2 infrared laser (wavelength: 10.6 μm; model: Universal Laser VLS 2.3.0) operated at 3.6 W power and 90 mm/s scan speed. These parameters were optimized based on preliminary tests to produce a continuous, fibrous, and conductive graphene network with typical sheet resistance values of 20–30 Ω/sq [15].

To improve LIG's strain resistance, we implemented two sequential treatments:

(1) Low-temperature annealing: The as-fabricated samples were annealed at 180°C for 4 minutes (AT 4) in a vacuum drying oven. The vacuum level was actively monitored and adjusted during heating to prevent oxidation of the carbon structure. This process promotes structural rearrangement and densification of the carbon network.

(2) Oxygen plasma etching: The annealed LIG samples were subjected to oxygen plasma using a GD-10 tabletop plasma cleaner (Shanghai Xuanyi Instruments) at 200 W for 25 minutes (ET 25) under 0.5 Torr. The etching process selectively removes loosely bonded or amorphous carbon, sharpens microstructures, and increases surface roughness for better interconnectivity.

Four experimental groups were defined: untreated LIG, AT 4 only LIG, ET 25 only LIG, and the dual-treated LIG (AT 4 followed by ET 25).

The schematic workflow and structural evolution during fabrication are illustrated in Figure 1. As shown in Figure 1a, CO_2 laser scribing locally pyrolyzes the PI substrate, generating conductive porous carbon networks that form the basis of LIG. The dual-treated process is detailed in Figure 1b, where the upper pathway corresponds to a single-step plasma-etched LIG, and the lower pathway shows the combined annealing and etching treatment that leads to the formation of the final fractal fiber structure.

Notably, Figure 1c illustrates the morphology of a single untreated LIG fiber with the dual-treated one. While conventional LIG fibers are loosely packed and linear, the dual-treated fibers form complex, interconnected fractal networks, which contribute to improved mechanical stability and resistance consistency under strain, and are characterized as fractal-fiber LIG (f-LIG).

Characterizations

Surface morphology was observed via SEM (Hitachi S-4800). Raman spectroscopy (Renishaw inVia, 532 nm laser) was used to assess structural defects and graphitization, with the D and G bands located near 1350 cm-1 and 1580 cm^{-1}, respectively. The I_D/I_G ratio was used to quantify disorder levels. XPS (Thermo Scientific K-Alpha) provided insight into bonding environments, including C–C, C–O, and C=O contents. Thickness was measured using a stylus profiler (Dektak XT).

Experimental Setup

Mechanical testing was performed by mounting samples onto a flexible polyacrylate substrate, then applying uniaxial tensile strain using a stepper-controlled displacement stage. Resistance was recorded in real-time using a Keithley 2450 Sourcemeter with a sampling rate of 300 S/s. Gauge factor (GF) was calculated using:

$$GF = \frac{\Delta R/R_0}{\varepsilon} \quad (1)$$

where R_0 is initial resistance and ε is applied strain.

To evaluate long-term durability and practical integration, transfer tests were performed by laminating treated LIG patterns onto PDMS-based stretchable substrates. Stretch–release cycles were applied while monitoring resistance to assess mechanical stability.

RESULTS AND DISCUSSION

Microstructural Evolution After Dual-Treatment

The morphological evolution of LIG under different treatments was systematically investigated via SEM. Figure 2a shows that untreated LIG exhibits a relatively open and porous morphology composed of loosely entangled carbon microfibers, with large voids and weak interconnectivity.

After oxygen plasma etching alone (ET 25), the LIG structure becomes rougher and more fragmented, as seen in Figure 2b. The etching process effectively removes some disordered or non-conductive carbon, but the structure

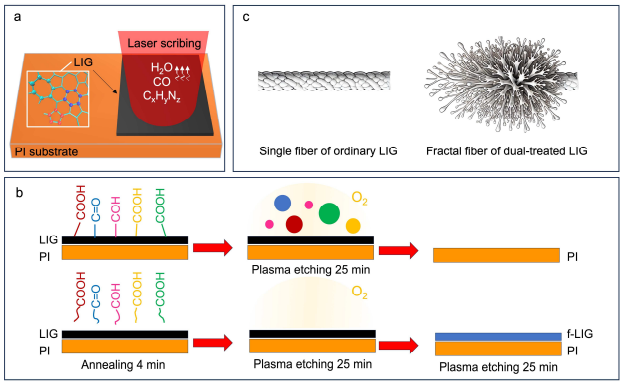

Figure 1: Fabrication process of f-LIG. (a) Schematic of laser scribing on a PI substrate using a 10.6 μm CO_2 infrared laser to form LIG patterns. (b) Schematic of dual-treated methods applied to LIG: the upper diagram shows LIG without annealing, ending after plasma etching; the lower diagram illustrates the process of applying AT 4 followed by ET 25 treatment. (c) Illustration of fractal fiber structure transformation.

remains fragile and discontinuous, leading to compromised electrical performance under strain.

Low-temperature annealing (AT 4) without etching, shown in Figure 2c, induces partial densification of the fibrous network. The fibers appear more compact and aligned, suggesting some degree of carbon reorganization. However, fiber–fiber junctions remain poorly connected, and mechanical reliability is still limited.

The dual-treated LIG, as illustrated in Figure 2d, exhibits a striking transformation into a fractal fiber structure. This architecture features densely packed microfibers with multiple branching pathways and increased interweaving. Such a configuration facilitates stress dispersion across multiple fiber junctions during stretching, thereby preventing abrupt electrical disconnection. The inter-fiber slippage enabled by the fractal nature provides additional flexibility, a key feature in soft electronic systems.

Graphitic Quality and Defect Density

To evaluate the structural ordering and defect levels in LIG after different treatments, Raman spectroscopy was conducted (Figure 2e). All samples exhibit two characteristic peaks: the D band (~1350 cm^{-1}), associated with structural defects and disordered carbon, and the G band (~1580 cm^{-1}), corresponding to the E_{2g} vibration mode in sp^2-hybridized graphitic domains. The intensity ratio of these peaks (I_D/I_G) is commonly used as an indicator of defect density in carbon-based materials [16].

Among the samples with different annealing durations (AT 4, AT 25, and AT 60), the AT 4 sample shows the lowest I_D/I_G ratio, indicating the highest graphitization level. In contrast, longer annealing times (25 and 60 minutes) lead to a slight increase in the I_D/I_G, suggesting that excessive annealing may reintroduce disorder, possibly due to stress accumulation or localized reoxidation. The untreated LIG shows the highest I_D/I_G value of 1.08, while the dual-treated sample exhibits a significantly reduced ratio of 0.79, confirming that the

combination of short-term annealing and plasma etching optimally reduces disorder while preserving sp^2 carbon networks.

XPS analysis further supports these observations. The C 1s spectra (Figure 2f,g) show that the relative content of C–C sp^2 bonds increases from 68.62% (untreated) to 78.85% (dual-treated) while oxygen-containing bonds (C-O and C=O) decrease. These results indicate effective deoxygenation and defect passivation, contributing to improved charge transport pathways. The reduction in oxygenated functional groups also implies enhanced environmental stability and reduced charge scattering.

Laser Energy Density Effects

The energy density of the laser plays a crucial role in determining the morphology and electrical performance of LIG. As shown in Figure 3a, increasing the laser energy density (E_d) results in thicker LIG films, characterized by a greater vertical height (W, W_1, W_2). Thicker LIG tends to exhibit lower sheet resistance due to increased conductive cross-section, as reflected in the data shown in Figure 3b. However, excessively high laser power may over-carbonize the PI surface, forming rigid, brittle graphitic layers with poor flexibility. SEM images in Figure 3c,d illustrate that LIG generated at E_d = 4.0 mJ/mm and P = 3.6 W retains a well-entangled fiber morphology, while higher power (P = 6 W) leads to a layered, plate-like structure. The fibrous configuration enables greater mechanical adaptability, which is crucial for flexible electronics. Therefore, a moderate 4.0 mJ/mm energy density was chosen as optimal to balance conductivity, surface morphology, and strain resilience.

Strain Resistance and Gauge Factor Improvement

The mechanical response of LIG electrodes under strain was tested by applying uniaxial tensile deformation up to 20% and monitoring resistance changes in real-time. As shown in Figure 4a, untreated and annealed AT 4-only samples demonstrate steep resistance increases under strain, corresponding to high GF (~14), which indicates high strain sensitivity but poor mechanical robustness.

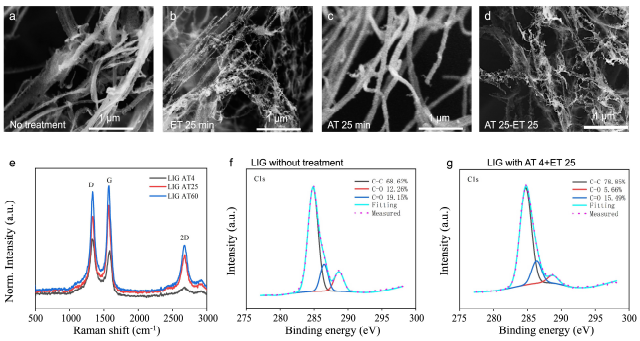

Figure 2: Morphological and chemical analysis of LIG under various treatments (a-d) SEM images showing LIG morphology: (a) untreated LIG (fibrous structure); (b) LIG after ET 25 treatment (fragile filamentous structure); (c) LIG after AT 4 treatment (dense fibrous structure); (d) LIG with combined AT 4 and ET 25 treatment (fractal fiber structure). (e) Raman spectra comparing different annealing treated LIG (4, 25, 60 min). (f) XPS C 1s spectra of untreated LIG. (g) XPS C 1s spectra of dual-treated LIG.

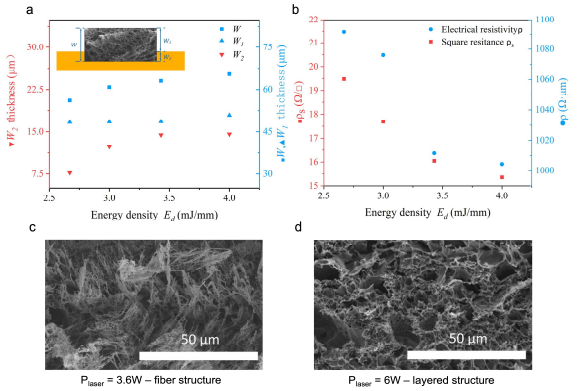

Figure 3: Analysis of LIG properties influenced by E_d. (a) Relationship between E_d and LIG thickness, including both the overall thickness and protruding heights (W, W_1, W_2). The Inset picture shows an SEM image highlighting the thickness measurement parameters. (b) Relationship between E_d and electrical properties shows trends in electrical resistivity ρ and square resistance ρ_s. (c) SEM image of LIG fabricated at E_d = 4.0 mJ/mm, P_{laser} = 3.6 W with a fiber structure. (d) SEM image of LIG fabricated at E_d = 4.0 mJ/mm, P_{laser} = 6 W with a layered structure.

In contrast, the dual-treated LIG maintains more stable resistance under identical strain, yielding a gauge factor of 7.43, which is approximately 50% lower than untreated LIG (Figure 4b). This performance enhancement reflects the structural benefits of the fractal microfiber network, which can stretch and deform without severely disrupting electrical pathways.

The reduced GF does not imply loss of sensitivity but rather indicates a more stable and predictable electrical response under dynamic conditions, a critical advantage for applications like soft sensors, stretchable interconnects, and wearable circuits.

Pattern Transfer and Repeatable Stretchability

Beyond mechanical resilience, we also evaluated the transferability and stretch-cycle endurance of LIG patterns.

Figure 4c shows that dual-treated LIG transfers cleanly onto PDMS, retaining sharp edges and intact patterns without residue. This is essential for integrating LIG into soft device platforms.

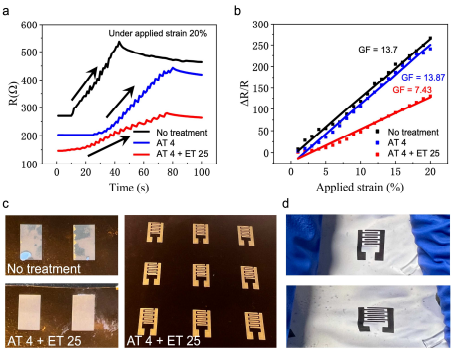

Figure 4: Strain performance and transfer quality of LIG samples. (a) Electrical performance of three 6 × 6 mm^2 LIG samples under progressively applied strain up to 20%. (b) GF comparison for the three LIG samples shown in (a). (c) Transferred LIG patterns with and without dual treated. (d) Stretching test of transferred LIG on flexible substrate.

Figure 4d demonstrates the stable resistance performance under repeated stretching, confirming the mechanical durability and adhesion of the transferred LIG. Even after multiple strain cycles, the resistance variation remains within 5%, suggesting excellent reliability for practical applications in skin-mounted electronics, soft robotics, and e-textiles.

CONCLUSIONS

We report a simple yet effective dual-treated method combining low-temperature annealing and oxygen plasma etching to enhance the strain resistance of laser-induced graphene. The process produces a robust fractal-fiber network with reduced defect density and improved conductivity retention under strain. Dual-treated LIG electrodes achieve a gauge factor of 7.43, half of that in the untreated counterparts, demonstrating superior flexibility and mechanical durability. This scalable strategy provides a practical route to high-performance, strain-resilient graphene-based electrodes for next-generation flexible electronics.

ACKNOWLEDGEMENTS

This work is supported by the Shenzhen Fundamental Research Funds (No. JCYJ20220530143011026). The authors thank the MEMS Lab at SIGS Tsinghua University for access to instrumentation—special thanks to Yixin Liu for valuable discussions!

REFERENCES

[1] T. S. D. Le, H. P. Phan, S. Kwon, S. Park, Y. Jung, J. Min, B. J. Chun, H. Yoon, S. H. Ko, S. W. Kim, and Y. J. Kim, "Recent advances in laser-induced graphene: Mechanism, fabrication, properties, and applications in flexible electronics," Adv. Funct. Mater., vol. 32, p. 2205158, 2022.

[2] F. M. Vivaldi, A. Dallinger, A. Bonini, N. Poma, L. Sembranti, D. Biagini, ... and F. Di Francesco, "Three-dimensional (3D) laser-induced graphene: Structure, properties, and application to chemical sensing," ACS Appl. Mater. Interfaces, vol. 13, no. 26, pp. 30245–30260, 2021.

[3] Y. Liu, Y. Chen, Z. Wang, and M. Zhang, "Enhanced electrical conductivity in laser-induced graphene-silicon carbide laminated nanosheets for flexible strain sensors and pulse wave velocity assessment," in Proc. IEEE Int. Conf. Micro Electro Mechanical Systems (MEMS), Jan. 2024, pp. 919–922.

[4] Y. Chen, Y. Liu, J. Liu, Y. Li, Y. Liu, W. Zhang, ... and M. Zhang, "Porous PDMS–ZnO wearable gas sensor for acetone biomarker detection and breath analysis," ACS Appl. Mater. Interfaces, vol. 16, no. 45, pp. 62436–62445, 2024.

[5] H. Yoon, K. Lee, H. Shin, S. Jeong, Y. Lee, S. Yang, and S. Lee, "In situ co-transformation of reduced graphene oxide embedded in laser-induced graphene and full-range on-body strain sensor," Adv. Funct. Mater., vol. 33, p. 2300322, 2023. DOI: 10.1002/adfm.202300322.

[6] L. Cheng, C. S. Yeung, L. Huang, G. Ye, J. Yan, W. Li, C. Yiu, F.-R. Chen, H. Shen, B. Z. Tang, Y. Ren, X. Yu, and R. Ye, "Flash healing of laser-induced graphene," Nat. Commun., vol. 15, Art. 2925, 2024. DOI: 10.1038/s41467-024-47341-1.

[7] J. Liu, D. Wu, C. Liu, Q. Wang, and H. Wang, "Full-range on-body strain sensor of laser-induced graphene embedded in thermoplastic elastomer via hot pressing transfer for monitoring of physiological signals," Adv. Mater. Technol., vol. 9, no. 1, p. 2301658, 2024. DOI: 10.1002/admt.202301658.

[8] F. Abedheydari, S. Sadeghzadeh, M. Saadatbakhsh, A. Heydariyan, and E. Khakpour, "Silver-decorated laser-induced graphene for a linear, sensitive, and almost hysteresis-free piezoresistive strain sensor," Sci. Rep., vol. 14, Art. 28715, 2024. DOI: 10.1038/s41598-024-80158-y.

[9] L. Yang, J. Yan, C. Meng, A. Dutta, X. Chen, Y. Xue, G. Niu, Y. Wang, S. Du, P. Zhou, C. Zhang, S. Guo, and H. Cheng, "Vanadium oxide-doped laser-induced graphene multi-parameter sensor to decouple soil nitrogen loss and temperature," Adv. Mater., vol. 35, no. 14, p. 2210322, 2023. DOI: 10.1002/adma.202210322.

[10] H. Wang, Z. Zhao, P. Liu, and X. Guo, "A soft and stretchable electronics using laser-induced graphene on polyimide/PDMS composite substrate," npj Flexible Electron., vol. 6, Art. 26, 2022. DOI: 10.1038/s41528-022-00161-z.

[11] A. M. Barja, Y. K. Ryu, S. Tarancon, E. Tejado, A. Hamada, A. Velasco, and J. Martinez, "Laser-induced graphene strain sensors for body movement monitoring," ACS Omega, vol. 9, no. 37, pp. 38359–38370, 2024. DOI: 10.1021/acsomega.3c09067.

[12] J. Ji, W. Zhao, Y. Wang, Q. Li, and G. Wang, "Templated laser-induced graphene-based tactile sensors enable wearable health monitoring and texture recognition via deep neural network," ACS Nano, vol. 17, no. 20, pp. 20153–20166, 2023. DOI: 10.1021/acsnano.3c05838.

[13] W. Wang, L. Lu, Z. Li, L. Lin, Z. Liang, X. Lu, and Y. Xie, "Fingerprint-inspired strain sensor with balanced sensitivity and strain range using laser-induced graphene," ACS Appl. Mater. Interfaces, vol. 14, no. 1, pp. 1315–1325, 2022. DOI: 10.1021/acsami.1c16646.

[14] M. Guan, Z. Zhang, W. Zhu, Y. Gao, S. Wang, and X. Li, "Femtosecond laser-induced graphene for temperature and ultrasensitive flexible strain sensing," Front. Mater. Sci., vol. 18, Art. 240696, 2024. DOI: 10.1007/s11706-024-0696-6.

[15] Y. Liu, H. Li, and M. Zhang, "Wireless Battery-Free Broad-Band Sensor for Wearable Multiple Physiological Measurement," ACS Appl. Electron. Mater., vol. 3, pp. 1681-1690, 2021.

[16] S. Eigler, C. Dotzer, and A. Hirsch, "Visualization of defect densities in reduced graphene oxide," Carbon, vol. 50, no. 10, pp. 3666–3673, 2012.

CONTACT

*Yanru Chen, tel: +1-858-412-9248;
yac054@ucsd.edu